



Assessing the sensitivity of the hydroxyl radical to model biases in composition and temperature using a single-column photochemical model for Lauder, New Zealand

L. López-Comí^{1,2}, O. Morgenstern^{1,*}, G. Zeng^{1,*}, S. L. Masters², R. R. Querel¹, and G. E. Nedoluha³

¹National Institute of Water and Atmospheric Research (NIWA), Lauder, New Zealand

²Department of Chemistry, University of Canterbury, Christchurch, New Zealand

³United States Naval Research Laboratory, Washington, DC, United States

*now at NIWA, Wellington, New Zealand

Correspondence to: O. Morgenstern (olaf.morgenstern@niwa.co.nz)

Abstract. We assess the major factors contributing to local biases in the hydroxyl radical (OH) as simulated by a global chemistry-climate model, using a single-column photochemical model (SCM) analysis. The SCM has been constructed to represent atmospheric chemistry at Lauder, New Zealand, which is representative of the background atmosphere of the Southern Hemisphere (SH) mid-latitudes. We use long-term observations of variables essential to tropospheric OH chemistry, i.e. ozone (O₃), water vapour (H₂O), methane (CH₄), carbon monoxide (CO), and temperature, and assess how using these measurements affect OH calculated in the SCM, relative to a reference simulation only using modelled fields. The analysis spans 1994 to 2010. Results show that OH responds approximately linearly to correcting biases in O₃, H₂O, CO, CH₄, and temperature. The biggest impact on OH is due to correcting H₂O, using radiosonde observations. This is followed by correcting O₃. Its impact is decomposed into a kinetics effect and a photolysis effect; both are of similar magnitude. The OH sensitivity to correcting CH₄ and CO biases is inversely related to the relative changes applied to these two species. The work demonstrates the feasibility of quantitatively assessing OH sensitivity to biases in longer-lived species, which can help to explain differences in simulated OH between global chemistry models and relative to observations. In addition to clear-sky simulations, we have performed idealised sensitivity simulations to assess the impact of clouds (ice and liquid) on OH. The results indicate that the impacts on the ozone photolysis rate and OH are substantial, with a general decrease of OH below the clouds relative to the clear-sky situation, and an increase above. The effects of liquid and ice clouds are less-than-additive. Using the SCM simulation we calculate recent OH trends at Lauder. For the period of 1994 to 2010, all trends are insignificant, in agreement with previous studies.



1 Introduction

The hydroxyl radical (OH) is essential to atmospheric chemistry as the leading atmospheric oxidant in the atmosphere. It acts as a “detergent”, reacting with numerous, mostly organic pollutants (Levy, 1971; Logan et al., 1981; Thompson, 1992; Lelieveld et al., 2004; Naik et al., 2013). Therefore, the oxidizing capacity of the atmosphere is largely determined by the abundance of OH radicals. Tropospheric ozone (O_3), an air pollutant and greenhouse gas (GHG), is the primary source of OH in the troposphere. It forms OH via O_3 photolysis yielding excited oxygen ($O(^1D)$) and a subsequent reaction of $O(^1D)$ with water vapour (H_2O). Stratospheric O_3 also plays an important role through its impact on the O_3 photolysis rate j_{O^1D} which is affected by the overhead O_3 column.

Due to its very short lifetime (the global lifetime is estimated to be ~ 1 s, Prinn, 2001; Elshorbany et al., 2012) and large variability, in-situ measurements of OH do not sufficiently constrain its global abundance (Heard and Pilling, 2003). OH is routinely included in global models of tropospheric chemistry, but the complexity of the tropospheric chemical system and the sensitivity of OH to a variety of environmental factors mean that there is considerable disagreement among global chemistry-transport and chemistry-climate models regarding the global OH abundance, often expressed in terms of the CH_4 lifetime (e.g., Stevenson et al., 2006; Naik et al., 2013).

A useful indirect method for determining global OH is based on tracking the abundance of long-lived, well-mixed chemicals for which oxidation by OH is the dominant sink and which have a well-quantified, industrial source. The most widely used such species is methyl chloroform (CH_3CCl_3) (Prinn et al., 2005). Montzka et al. (2011) use CH_3CCl_3 measurements to infer only a small inter-annual variation in OH for 1998-2007. A further indirect method to address OH is to measure ^{14}CO (Manning et al., 2005). Krol et al. (2008) find some considerable variability but no long-term trend using this method.

Addressing the uncertainty in modelling OH in global models sometimes involves juxtaposing them to local-scale (box or single-column) models constrained by observations and incorporating only the fast photochemical processes (Emmerson et al., 2005, 2007). In the present paper, we introduce and evaluate a single-column model (SCM) constrained with available long-term observations at Lauder, New Zealand ($45^\circ S$, $170^\circ E$, 370 m above sea level). Lauder is known for its clean air, large diversity of available measurements, and, for several of them, long time series, so is ideal for this kind of study. The SCM is built around a medium-complexity stratosphere-troposphere chemistry scheme. The model is forced with Lauder observations and/or output from a chemistry-climate model that uses the same scheme (see below). In Section 1, we describe the set-up of the SCM, the construction of time series of key species and meteorological parameters that drive the SCM, and the simulations. In Section 3, we present results of simulated OH concentrations and trends from the SCM and analyse the sensitivity of OH to various forcings. Conclusions are gathered in Section 4.



2 Models and simulations

2.1 The single-column photochemical model (SCM)

The single-column photochemical model (SCM) is a stand-alone version of the stratosphere-tropo-
60 sphere chemistry mechanism used by the NIWA-United Kingdom Chemistry and Aerosol (NIWA-
UKCA) model, which comprises gas-phase photochemical reactions relevant to the troposphere and
stratosphere (Morgenstern et al., 2009, 2013; Telford et al., 2013; O'Connor et al., 2014). The 60
vertical levels of the SCM are the same as in NIWA-UKCA, extending to 84 km. Unlike NIWA-
UKCA, the SCM excludes all non-chemistry processes, such as transport, dynamics, the boundary-
65 layer scheme, radiation, emissions, etc. This means the model is only suitable for assessing fast
photochemistry.

Morgenstern et al. (2013) and O'Connor et al. (2014) describe the chemistry scheme included in
the SCM. The SCM includes an isoprene oxidation scheme (Pöschl et al., 2000; Zeng et al., 2008)
not included in the NIWA-UKCA model version used by Morgenstern et al. (2013). In addition to
70 CH₄ and CO, the model includes a number of primary non-methane volatile organic compound
(NMVOC) source gases, i.e. ethane (C₂H₆), propane (C₃H₈), acetone (CH₃COCH₃), formalde-
hyde (HCHO), acetaldehyde (CH₃CHO), and isoprene (C₅H₈). As noted above, emission and de-
position of species are not considered in the SCM. The SCM includes a comprehensive formulation
of stratospheric chemistry (Morgenstern et al., 2009) comprising bromine and chlorine chemistry
75 and heterogeneous processes on liquid sulfate aerosols. Overall, the model represents 86 chemical
species and 291 reactions including 59 photolysis and 5 heterogeneous reactions. The FAST-JX
interactive photolysis scheme (Neu et al., 2007; Telford et al., 2013) has been implemented in the
SCM. The chemical integration is organised through a self-contained atmospheric chemistry pack-
age (Carver et al., 1997), and the differential equations describing chemical kinetics are solved using
80 a Newton-Raphson solver (Morgenstern et al., 2009).

2.2 Construction of vertical profiles of forcing species and meteorological parameters

Time series of O₃, H₂O, CO, and temperature profiles are produced using mainly long-term mea-
surements from Lauder, supplemented with NIWA-UKCA results as detailed below. Lauder is a
member of several international networks, including the Network for the Detection of Atmospheric
85 Composition Change (NDACC; <http://www.ndsc.ncep.noaa.gov>), the Global Reference Upper Air
Network (GRUAN; <http://www.gruan.org>), and Global Atmosphere Watch (GAW; http://www.wmo.int/pages/prog/arep/gaw/gaw_home_en.html), where these data are archived and made available.
The networks coordinate long-term observations of O₃, various other constituents, and meteorolog-
ical parameters. Here we briefly describe the procedure of constructing forcing data, using Lauder
90 observations, to be used to constrain the SCM. The resulting profiles are shown in Fig. 1.



O₃ profiles used here are a combination of ozonesonde time series (from the surface to 25 km, Bodeker et al., 1998) combined with the Microwave Ozone Profiler Instrument 1 (MOPI1) time series for altitudes above 25 km (Boyd et al., 2007; Nedoluha et al., 2015), covering 1994 to 2010 (Fig. S1a). The ozone sondes have been launched approximately weekly; this defines the temporal coverage of the forcing data used in the SCM calculations. Microwave measurements used here come as several profiles a day at a variable spacing; we interpolate them to the ozone sonde launch times. Any missing data (during the two periods when the microwave instrument was out of service) are filled using a Fourier series gap-filling method. We compare the two datasets in the height region usefully covered by both (20 to 30 km). The differences between the two measurements range between -2% and +6%, and a mean bias that is less than 5%. O₃ profiles are linearly interpolated onto the SCM's grid. Vertically integrated ozone produced here is also compared to total-column ozone measured by the Lauder Dobson instrument; the difference is about 5% on average (López Comí, 2016). Lauder ozone measurements have been used in various World Meteorological Organization (WMO) ozone assessments (e.g., WMO, 2011).

H₂O profiles have been constructed using the weekly radiosonde measurements of H₂O vapour below 8 km (the same soundings that also measure ozone) and NIWA-UKCA model output data above. For validation, we use the monthly National Atmospheric and Oceanic Administration (NOAA) Frost Point Hygrometer (FPH) H₂O vapour measurements (Vömel et al., 2007; Hall et al., 2016) which start in 2003. FPHs are more accurate compared to radiosonde hygrometers, particularly for stratospheric conditions. However, due to the later start of the FPH time series and the lower measurement frequency, radiosonde measurements are used in this study. The comparison of FPH and radiosonde H₂O reveals differences that are generally less than ±5% in the lower and middle troposphere but increase in and above the tropopause region (~ 11 km, López Comí, 2016). The radiosonde hygrometers have some known problems with measuring low humidity (Miloshevich et al., 2001). We therefore use radiosonde data up to 8 km of altitude, and NIWA-UKCA output above that.

We use surface in-situ measurements from Cape Grim, Tasmania (Cunnold et al., 2002) to rescale NIWA-UKCA model profiles, producing CH₄ profiles that coincide with the ozone sonde launches. The NIWA-UKCA model simulation had been constrained with historical global-mean surface CH₄ values, resulting in an overestimation relative to the Cape Grim data by ~ 2% (not shown), and both data show a ~ 5% increase in CH₄ at the surface over the period between 1994 and 2010. Cape Grim CH₄ is a good surrogate for the Lauder measurements because CH₄ is a long-lived, well-mixed atmospheric constituent.

The time series of CO profile over the period of 1994-2010 has been constructed using the NIWA-UKCA CO profiles, rescaled such that the total columns match those obtained from the mid-infrared Fourier Transform Spectrometer (FTS) at Lauder (Rinsland et al., 1998; Zeng et al., 2012; Morgenstern et al., 2012). Gaps in the total-column FTS series, such as the period between 1994 and 1996



when the FTS measurements had not started yet, are filled using a regression fit accounting for the mean annual cycle (modelled as a 6-term harmonic series) and the linear trend.

The time series of temperature profiles are constructed following the same procedure as used in
130 the construction of O_3 profiles, comprising the radiosonde temperature profiles (from the surface to 25 km) merged with microwave radiometer temperatures (above 25 km) for the period of 1994-2010.

2.3 Simulations

We perform SCM simulations covering the period of 1994-2010, summarized in Table 1. The forcing data needed by the SCM consist of profile series of temperature, pressure, optionally cloud liquid
135 and ice mass mixing ratios, and the mixing ratios of 86 chemical compounds. With the exceptions detailed below, these fields and species are taken from a NIWA-UKCA simulation for the period of 1994-2010, interpolated to the times of the ozone sonde launches. The CCM simulation used here consists of the last 17 years of a NIWA-UKCA "REF-C1" simulation conducted for the Chemistry-Climate Model Initiative (CCMI; Eyring et al., 2013). REF-C1 is a hindcast simulation for the period
140 of 1950 to 2010, using prescribed Hadley Centre sea Ice and Sea Surface Temperature (HadISST) fields (Rayner et al., 2003). The surface emissions of primary species are as described in Eyring et al. (2013), ozone-depleting substances (ODSs) follow the A1 scenario of the World Meteorological Organisation (WMO) Report (WMO, 2011), and surface (or bulk, in the case of CO_2) abundances of greenhouse gases (GHGs) follow the "historical" Intergovernmental Panel on Climate Change
145 (IPCC) scenario of global-mean GHG mixing ratios (Meinshausen et al., 2011).

In a "reference" simulation of the SCM all forcings are taken from this REF-C1 simulation of NIWA-UKCA. Alternatively, in sensitivity simulations O_3 , H_2O , CH_4 , CO , and temperature, or all of these simultaneously, are replaced with the time series of the profiles that are constructed using long-term observational data as described above. For species other than those 5 fields, in all cases
150 we use NIWA-UKCA REF-C1 forcings. We evaluate the SCM only for those times, spaced roughly weekly, for which ozone sonde data are available. With the exceptions of those simulations assessing cloud influences, simulations are conducted assuming clear-sky conditions.

3 OH sensitivity to correcting chemistry-climate model biases

In this section, we present sensitivity studies to assess the contribution of biases in known factors
155 (O_3 , H_2O , CH_4 , CO , and temperature) affecting OH photochemistry at Lauder. The response of OH to changes in each forcing is assessed individually and also in combination.

3.1 OH sensitivity to O_3 biases

Three sensitivity simulations are conducted to quantify the impact of O_3 biases (defined as differences between observed O_3 and NIWA-UKCA simulated O_3) on OH at Lauder.



160 As discussed above, the rate of production P of HO_x via $\text{O}(^1\text{D}) + \text{H}_2\text{O}$ can be expressed as

$$P(\text{HO}_x) \approx \frac{2kj_{\text{O}^1\text{D}}[\text{O}_3][\text{H}_2\text{O}]}{a[\text{O}_2] + b[\text{N}_2] + k[\text{H}_2\text{O}]} \quad (1)$$

where k is the rate efficient for $\text{O}(^1\text{D}) + \text{H}_2\text{O}$, $j_{\text{O}^1\text{D}}$ is the rate of O_3 photolysis producing $\text{O}(^1\text{D})$, and a and b are the rate coefficients of quenching of $\text{O}(^1\text{D})$ with O_2 and N_2 , respectively (Liu and Trainer, 1988; Thompson et al., 1989; Madronich and Granier, 1992; Fuglestedt et al., 1994).

165 Accordingly, $P(\text{HO}_x)$ is affected by ozone changes principally in two different ways: Either locally through a change in $[\text{O}_3]$ or non-locally through a change in $j_{\text{O}^1\text{D}}$ caused by changes in the overhead total-column ozone (TCO). To separate the effects, we conduct three simulations with the SCM: The first simulation targets the local kinetics effect by applying changes in O_3 concentrations but keeping all photolysis rates unchanged versus the reference simulation. A second simulation involves apply-
 170 ing changes in $j_{\text{O}^1\text{D}}$ according to changes in O_3 (keeping the rest of photolysis rates unchanged), but considering a fixed O_3 concentration, i.e. using the O_3 concentrations of the reference simulation. A third simulation includes both effects simultaneously.

The results of these three sensitivity runs are displayed in Fig. 2. As expected, the pattern of O_3 differences (Fig. 2a) is reflected in the pattern of OH differences (Fig. 2b), with increases of ozone
 175 in spring and decreases in autumn, relative to the reference simulation, resulting in changes of the same sign in OH. However, there is a height dependence to this relationship. The largest impact is in the free troposphere where these differences vary with altitude. In summer and autumn, O_3 biases range between -5% and -45% , meaning that the reference simulation overestimates the observations. Such a bias in O_3 results in up to 12% reductions in OH for these seasons when the
 180 bias is corrected. In spring, observed O_3 is larger than in the reference simulation by up to 10%. Consequently, this results in a $\sim 5\%$ increase of OH.

Regarding the sensitivity simulation considering the photolysis effects, $j_{\text{O}^1\text{D}}$ exhibits differences relative to the reference simulation ranging from $\sim 14\%$ to $\sim 30\%$. The corrections are positive everywhere, in accordance with the overestimation of TCO in the NIWA-UKCA model with respect
 185 to observations (Morgenstern et al., 2013; Stone et al., 2016). Therefore, the OH increases in Fig. 2(d) are the result of increases in $j_{\text{O}^1\text{D}}$ (Fig. 2c). The relative OH response is approximately 50% of the $j_{\text{O}^1\text{D}}$ relative difference. However, Figs. 2(c) and (d) suggest that the magnitudes of the kinetics and the photolysis effects, for the O_3 bias found at Lauder, are comparable.

OH resulting from the combined kinetics and photolysis effects is displayed in Fig. 2(e). OH
 190 responds approximately linearly to the two effects combined, compared to the sum of their individual impacts (Fig. 2f), despite some small differences between Fig. 2(e) and (f).

Next, we examine the relationship between slant column of O_3 (SCO), $j_{\text{O}^1\text{D}}$, and OH. Fig. 3(a) shows that there is an approximately exponential relationship between $j_{\text{O}^1\text{D}}$ and the SCO at 6 km of altitude (this effect also exists at other altitudes). The small curvature may be the result of inac-
 195 curately diagnosing the SCO (ignoring the curvature of the Earth). Another reason could be that the



cross section of O_3 is wavelength dependent, and consequently the actinic flux spectrum moves towards longer wavelengths with increasing SCO. j_{O^1D} and the OH concentration exhibit an approximately linear relationship (fig. 3b). Combining these results, we derive an approximately exponential relationship between the SCO and the OH concentration (fig. 3c).

200 To determine a simple coefficient that describes the quantitative contribution of O_3 to OH, a linear regression between differences in OH and O_3 relative to the reference was conducted through the following expression (note that this equation is also used to derive the linear contributions of the other key species to OH chemistry at Lauder):

$$\frac{\Delta[\text{OH}]}{[\text{OH}]_{ref}} = A_i \frac{\Delta X}{X_{ref}} \quad (2)$$

205 where X is the perturbation variable (in this case $[O_3]$), A_i is the slope of the linear regression, $\Delta[\text{OH}]$ is the absolute difference between the OH concentrations in the reference and perturbation simulations, ΔX is the absolute difference in concentrations of the perturbation variable X between the observations and the reference, $[\text{OH}]_{ref}$ is the OH concentration obtained from the reference simulation, and X_{ref} is the concentration of the reference variable. The regression coefficients A_i
 210 represent the sensitivity of OH to changes in each individual variable for the troposphere at Lauder. The regression coefficients are depicted in Fig. 4.

The sensitivity coefficients of OH to the kinetics and photolysis effects of O_3 are shown in Fig. 4(a). Coefficient A_1 , which represent the kinetics effect, ranges from 0 to 25% (meaning the relative response of OH is up to a quarter of the relative difference in O_3). The sensitivity to photolysis (A'_1)
 215 is $> 50\%$ throughout much of the troposphere (meaning the relative response in OH is over half the relative change in j_{O^1D}).

3.2 OH sensitivity to H_2O biases

A perturbation simulation was performed using combined radiosonde and NIWA-UKCA H_2O (section 2.2). The OH response to correcting H_2O biases (Fig. 5) shows an approximately linear response
 220 with respect to the relative changes in H_2O , i.e. decreases in H_2O generally lead to a reduction of OH concentrations (eq. 1). Note that NIWA-UKCA substantially overestimates the radiosonde-observed H_2O vapour by up to 60% between 2 and 6 km (Fig. 5a); this translates into an overestimation of OH by up to $\sim 40\%$ in the reference simulation (Fig. 5c) in the same region. The sensitivity of OH to changes in H_2O (eq. 2) range from 5 to 50% in the troposphere (Figs. 5e and 4 (b) coefficient
 225 A_2), with high sensitivity in the lower and free troposphere and reduced sensitivity in the tropopause region.

It is known that large uncertainties are associated with H_2O vapour measurements. To illustrate this, we repeat the above simulation but now using European Centre for Medium-Range Weather Forecasts (ECMWF) ERA-Interim re-analysis (hereafter ERAI) (Dee et al, 2011) H_2O . Irrespec-
 230 tively of the large differences and the opposite signs in H_2O biases between Lauder radiosonde and



ERA-Interim (ERA-Interim) data, the OH response to biases in H₂O show approximately the same linear relationship in both cases (Fig. 5). Likewise, the sensitivity of OH to changes in H₂O using ERA-Interim data (Figs. 5f and 4b, coefficient A_3) resembles the sensitivity simulation using radiosonde H₂O.

3.3 OH sensitivity to CH₄ and CO biases

235 The effect of CH₄ changes on OH is displayed in Fig. 6 (a,c,e). The CH₄ biases are generally small, up to only ~2%, and are assumed to be vertically uniform, with some seasonal variations. Decreases in CH₄ lead to increases in OH due to reduced loss of HO_x by CH₄ + OH. The response of OH to CH₄ changes maximizes around 2 km, and decreases at higher altitudes. The seasonal variation of the OH response to CH₄ biases maximizes in March/April (Fig. 6c), which coincides
240 with the maximum bias in CH₄ (Fig. 6a) in the same months. However, the sensitivity of OH to CH₄ changes maximizes in May/June (Fig. 6e), with a peak value of ~40%. The sensitivity coefficient describing the dependence of OH to CH₄ changes (denoted as A_4 in Fig. 4c) ranges from -0.17 at the surface to -0.35 at ~2 km of altitude, and then decreases to -0.15 at 10 km.

The CO bias and the resulting differences in OH are displayed in Fig. 6(b,d,f). The relative dif-
245 ference of OH with respect to the reference simulation is less than ±5% for all seasons (Fig. 6d), showing that decreases in CO generally lead to increases in OH through the reduced loss of OH through OH + CO. Note that during austral spring NIWA-UKCA overestimates CO, presumably due to exaggerated tropical biomass burning in the model which causes CO biases of up to 10% (Fig. 6b). The sensitivity of OH to changes in CO shown in Fig. 6(f) varies from -30 to -50%
250 and in absolute terms increases with altitude (the white band shown in October is the result of CO differences being close to zero).

The sensitivities of OH to CH₄ and CO show comparable values at the surface, but the OH sensitivity to CO increases with height whereas its sensitivity to CH₄ decreases. Note that the CH₄ + OH reaction rate is strongly temperature dependent, which may contribute to the lower sensitivity of OH
255 to CH₄ changes at altitude than to CO. However, further investigation will need to investigate how these ratios change in different chemical regimes, and to assess whether the relative sensitivity of OH to CO and to CH₄ are specific to the clean Southern-Hemisphere environment.

3.4 OH sensitivity to temperature biases

To assess the effects of changes in temperature on OH, we apply the same procedure as for O₃,
260 for which the effects of temperature have been decomposed into kinetics and photolysis effects. We perform three simulations: In the first simulation, we only apply temperature changes to chemical kinetics, keeping all photolysis rates fixed (noting that most uni-, bi-, and termolecular reaction rates are temperature dependent). In the second simulation, we only consider the photolysis effect, which arises mainly because the cross section of O₃, the primary UV absorber, is temperature dependent.
265 The impact of temperature on OH via ozone photolysis again occurs via two different mechanisms:



firstly, the changes in j_{O^1D} caused by changes in the actinic flux which relates to changes in the atmospheric transmissivity in the UV (caused by a temperature dependence of the cross section of overhead ozone), and the local changes of j_{O^1D} , due to the local temperature dependence of the ozone cross section. Here, we only evaluate the combined photolysis effect in the second simulation. Finally, we perform a third simulation by applying both the kinetics and the photolysis effects simultaneously.

At Lauder, the reference simulation is generally cold-biased (i.e., the temperature correction is positive; fig. 7a). This is particularly the case in the lowest 2 km and throughout the troposphere in the autumn-winter season. The kinetics effect leads to a reduction of OH by up to 2% (fig. 7b). $O(^1D) + H_2O$ and the quenching reactions (eq. 1) are not or weakly explicitly temperature dependent, making $CH_4 + OH$ (which is much more sensitive to temperature) the leading factor in causing this small OH reduction. The photolysis effect is often somewhat larger than the kinetics effect but peaks in spring (fig. 7c). This translates into a slight OH reduction comparable in magnitude to the kinetics effect (fig. 7d). Both effects add nearly completely linearly in the combined simulation (fig. 7e,f).

We calculate sensitivity coefficients A_6 and A_6'' that define the OH responses to both effects (fig. 4 e,f). Coefficient A_6 represents the kinetics effect and varies from 0 to -1.75 (i.e., in absolute terms, the relative OH response can be larger than the relative difference in T). The sensitivity coefficient that describes the sensitivity of OH to changes in photolysis (A_6'') ranges from 60% at the surface to 0% at 10 km of altitude. Figure 4 (e,f) shows sensitivity coefficients for both effects (A_6 and A_6''). OH changes due to both effects are small (up to 2.5%) and comparable in magnitude.

Several sensitivity studies have been conducted previously to elucidate the impact of temperature on OH (Stevenson et al., 2000; Wild, 2007; O'Connor et al., 2009). None of these studies separately assessed the impacts of the kinetics and photolysis effects of temperature on OH. Wild (2007) applied a globally uniform temperature rise of 5K that led to a larger OH abundance and an around 10% decrease in the CH_4 lifetime. O'Connor et al. (2009) showed a small impact on global OH abundances due to temperature biases; this may be because the temperature biases in their model were both positive and negative, in different regions, leading to some cancellation of the impact on global OH. Here, bias-correcting temperature is shown to have only a small impact on OH abundance (Fig. 7e); this result broadly corroborates that of O'Connor et al. (2009).

3.5 Linearity of OH sensitivity to biases in all forcings

Here, we assess the effect of changing all forcings (O_3 , H_2O , CH_4 , CO, and temperature) simultaneously on OH at Lauder. Fig. 8(a) shows the responses of OH to changing all forcings. A comparison with fig. 5 suggests that H_2O changes dominate the total response of OH to changes in these forcings. At Lauder, NIWA-UKCA is too moist (relative to radiosonde water vapour); this translates into a large OH overestimation of up to $\sim 40\%$ in the reference simulation (Fig. 8a). This is consistent



with the underestimated CH₄ lifetime by the NIWA-UKCA model (Morgenstern et al., 2013; Telford et al., 2013), assuming that the NIWA-UKCA model is too moist also in other regions. In general, in the SCM OH responds approximately linearly to the combined changes in major forcings that play an important role in OH chemistry (Fig. 8).

To examine the linearity of OH responses to simultaneous changes in key forcings defined in this study, the combination of all individual contributions, i.e. O₃ (kinetics and photolysis effects), H₂O, CH₄, CO, and temperature (kinetics and photolysis effects) to OH, was compared to the OH response to all forcings combined simulation in the SCM through Eq. (3):

$$\begin{aligned} 310 \quad \frac{\Delta[\text{OH}]}{[\text{OH}]_{\text{ref}}} \approx & A_1 \frac{\Delta[\text{O}_3]}{[\text{O}_3]_{\text{ref}}} + A_1'' \frac{\Delta j\text{O}({}^1\text{D})_{\text{O}_3}}{j\text{O}({}^1\text{D})_{\text{ref}}} + A_2 \frac{\Delta[\text{H}_2\text{O}]}{[\text{H}_2\text{O}]_{\text{ref}}} + A_4 \frac{\Delta[\text{CH}_4]}{[\text{CH}_4]_{\text{ref}}} + A_5 \frac{\Delta[\text{CO}]}{[\text{CO}]_{\text{ref}}} \\ & + A_6 \frac{\Delta T}{T_{\text{ref}}} + A_6'' \frac{\Delta j\text{O}({}^1\text{D})_{\text{T}}}{j\text{O}({}^1\text{D})_{\text{ref}}} \end{aligned} \quad (3)$$

where $\frac{\Delta[\text{OH}]}{[\text{OH}]_{\text{ref}}}$ is the relative difference in the OH concentration obtained with the SCM with respect to the reference simulation, using all forcings combined. The forcings comprise the kinetics and photolysis effects of O₃ (A_1 and A_1''), radiosonde H₂O (A_2), CH₄ (A_4), CO (A_5), and the kinetics and photolysis effects of temperature (A_6 and A_6'').

Eq. (3) describes the relationship between the single-perturbation experiments and the all-forcings simulation, assuming that the OH response is linear to changes in the forcings. Figure 8 indicates that the model responds approximately linearly to the combinations of all forcings, with OH responses in the all-forcings simulation correlating at 0.9 with the sum of the OH responses in the individual-forcing simulations. Fig. 8(c) however also suggests that there are some notable non-linearities in the system.

3.6 Trends in OH

We examine variability and trends in OH using the SCM simulation including all key forcings separately for different altitude bands. The results (Fig. 9) indicate that there are no significant trends in OH throughout the troposphere for the period of the simulation (1994-2010), but there is substantial interannual variability. This is in agreement with other studies (e.g., Manning et al., 2005; Montzka et al., 2011).

3.7 OH sensitivity to the presence of clouds

We have assessed the OH sensitivity to correcting biases in key forcings assuming clear sky. Here we explore the impact of simulated clouds on OH, recognizing that this process is associated with large uncertainties due to difficulties with representing clouds in models. Measurements of cloud profiles do not exist at Lauder, hence a bias correction like that performed with the composition and temperature fields is not possible. Therefore, here we only examine the impact of clouds simulated



by NIWA-UKCA on j_{O^1D} and OH at Lauder, relative to the clear-sky reference simulation used
335 before. The impacts of liquid water clouds (LWCs) and ice clouds (ICs) were assessed separately
and combinedly. Three simulations are defined here, i.e. (1) including only ICs, (2) including only
LWCs, and (3) considering both combined (LICs).

Fig. 10(a,c,e) shows the response of j_{O^1D} and OH to the presence of the ICs. j_{O^1D} and OH are
generally reduced below the ICs, relative to the cloud-free situation. The maximum reduction in OH
340 is 10 to 15% in winter below 2 km, coinciding with the maximum reduction in j_{O^1D} . There are
increases in both fields (up to $\sim 8\%$) above the ICs in austral spring, associated with the seasonal
peak in IC occurrence at the same time. In general, j_{O^1D} and OH impacts vary strongly with season,
with the maximum reduction occurring in winter close to the surface, and the maximum increase in
spring above the ICs.

345 LWCs are mostly present between 1 and 4 km with the seasonal peak in austral spring (fig. 10b).
Similarly to ICs, j_{O^1D} and OH are enhanced above and throughout much of the cloud layer, and
reduced in the lowest 1 km above the surface (fig. 10e,g). The enhancement in j_{O^1D} and OH peaks
at 12% between 2 and 4 km of altitude, coinciding with the spring maximum in liquid water content
at 1–2 km. Conversely, the reduction in j_{O^1D} and OH with respect to the clear-sky condition is
350 $\sim 10\%$ and is produced below the clouds.

The simulation with the combined effect of ICs and LWCs (LICs) produces a reduction in j_{O^1D}
and OH that ranges between 0% and 20% below the transition of ICs to LWCs at around 2 km, since
LWCs are as much as twice as optically dense as ICs (fig. 10g). An enhancement is produced above
this altitude of up to 18%. The magnitudes of changes in j_{O^1D} and OH are similar when either ICs
355 or LWCs are considered in the SCM. Furthermore, their effects add up slightly less than linearly
when both are present in the simulations (fig. 10h).

The results shown here indicate that lower clouds generally produce an enhancement in j_{O^1D}
(Fig. 10d), but higher clouds generally produce a reduction in j_{O^1D} in the free troposphere (Fig.
10b; Tang et al., 2003; Tie et al., 2003; Liu et al., 2009). Furthermore, the vertically and seasonally
360 averaged enhancement and reduction in j_{O^1D} are about 2% and 6% respectively for the LWC clouds,
similar to the response for the ICs condition; this suggests that the cloud vertical distribution has a
bigger effect on photolysis than the change in cloud water content (Tie et al., 2003).

4 Conclusions

The sensitivity of the OH abundance at Lauder to NIWA-UKCA model biases in key forcing vari-
365 ables (O_3 , H_2O , CH_4 , CO , and temperature) have been quantified for clear-sky conditions, using a
single-column model (SCM). Only fast photochemistry is represented in the SCM; slow chemistry,
transport, and other physical processes are thus not considered. The bias-corrected profiles of the key
forcing variables have been constructed largely using long-term Lauder measurements, combined



with NIWA-UKCA output. Also a few other sources of data (Cape Grim methane measurements,
370 ERA-Interim water vapour) have been used.

The results show that OH responds approximately linearly to correcting biases in O_3 , H_2O , CH_4 ,
CO, and temperature. We have decomposed the OH response to O_3 changes into the kinetic effect
(i.e. local impacts on the chemical equilibrium of changing $[O_3]$) and the photolysis effect (as medi-
ated by changes in the overhead O_3 column affecting photolysis rates). We find that the kinetic effect
375 of correcting positive biases in modelled O_3 causes a reduction in OH during austral summer and
autumn (by up to 20% at 7 km), and an increase in the free troposphere in austral spring (of > 5% in
October at 3 km); such changes in OH are nearly linearly related to the corresponding ozone biases.
NIWA-UKCA generally overestimates the ozone column. Correcting this effect causes j_{OD} to in-
crease by 15 – 30% below 10 km, causing general OH increases which maximize at around 16%
380 between 2 and 6 km in summer. The model responds approximately linearly to the combined effects
of photolysis and kinetics.

NIWA-UKCA considerably overestimates the H_2O vapour concentration compared to radiosonde
measurements. Correcting this moist bias leads to > 34% reductions in OH in the free troposphere
during the austral summer. The sensitivity coefficient of OH to biases in H_2O vapour is relatively
385 large in the lower troposphere but decreases with altitude. Assuming this moist bias is not restricted
to Lauder (which we do not assess here), this is thus a leading explanation for NIWA-UKCA to
produce an underestimated CH_4 lifetime, relative to accepted literature estimates.

The bias in modelled CH_4 is small since surface CH_4 in the SCM reference simulation is con-
strained to follow globally averaged surface observations. The Southern Hemisphere generally has a
390 slightly smaller CH_4 burden than the North. Correcting the resulting positive bias at Lauder causes
increases in OH throughout the troposphere, with a seasonal peak in March/April. OH is most sen-
sitive to CH_4 changes in winter, though. In the analysis of the OH sensitivity to CH_4 , the impact of
subsequent changes in CH_4 oxidation products which also affect OH could not be addressed within
the constraints of an SCM. Inclusion of this effect could change the sensitivity coefficient for CH_4
395 (Spivakovsky et al., 2000).

Except for October-December, NIWA-UKCA has a tendency to underestimate CO. As with CH_4 ,
the sensitivity of OH to changes in CO is negative throughout the troposphere, reflecting that
CO + OH is an important sink for OH.

We show that OH responds linearly to temperature biases. These effects cause a small reduction
400 in OH due to the strong dependence of OH + CH_4 on temperature. However, for NIWA-UKCA the
impact of temperature biases on OH at Lauder is small, in agreement with O'Connor et al. (2009).

The results of the simulation considering simultaneous changes in all the key forcings indicate
that OH responds approximately linearly to all the major forcings that contribute to the oxidising
capacity of the atmosphere. We find that biases in O_3 , H_2O , CH_4 , CO, and temperature all affect the
405 oxidising capacity of the atmosphere at Lauder, with H_2O and O_3 biases dominating. The NIWA-



UKCA model generally produces a moist bias (by $\sim 0 - 50\%$) relative to radiosonde measurements; this leads to an overestimation of OH of up to 40%. This makes water vapour a leading contender to explain the underestimated global lifetime of CH_4 in NIWA-UKCA (Morgenstern et al., 2013; Telford et al., 2013). We find no significant trend in OH over Lauder over the period 1994-2010.

410 The SCM approach can be applied to other parts of the globe where reliable long-term observations of O_3 and H_2O exist. In-situ observations of CH_4 and CO are not that critical; CH_4 can be estimated from non-local measurements, and relatively reliable satellite measurements of total-column CO exist (e.g., Pan et al., 1995; Morgenstern et al., 2012). However, in polluted regions, such as in much of the Northern Hemisphere, NO_x and NMVOC levels are elevated relative to Lauder and
415 affect in-situ ozone production. This means that these constituents might need to be bias-corrected if the SCM is applied in such regions. This might affect the suitability of our approach under these conditions.

Having determined the contributions of the major forcings to the chemistry of OH at Lauder under clear-sky conditions, a step forward would be to assess the impact of clouds on photolysis and thus
420 OH, which could be substantial. Due to a lack of suitable observations to constrain the SCM model with cloud profiles at Lauder, we only assessed how the presence of modelled cloud affects OH, relative to the clear-sky situation. The results show that OH response to cloud strongly depends on the vertical distribution of the clouds, not just the total amount. Both liquid- and ice clouds lead to increases in OH above and to some extent inside the cloud, particularly in the spring season when
425 this effect maximizes. Considering that clouds are amongst the most difficult aspects of the climate system to model adequately, we stipulate that observational profiles of cloud properties would be highly desirable to use for a future continuation of this line of research.

In summary, we conclude that at Lauder, OH modelled in NIWA-UKCA is most sensitive to issues with representing water vapour and ozone. This points to the need to improve representations
430 of the hydrological cycle and of tropospheric and stratospheric ozone chemistry in NIWA-UKCA and possibly other, similar chemistry-climate models.

Author contributions

O. Morgenstern devised the original idea. L. López Comí wrote the model, conducted the simulations, performed the data analysis, and led the writing of the paper, with support from S. Masters, O.
435 Morgenstern, and G. Zeng. G. Nedoluha contributed the microwave ozone data to the research; R. Querel contributed the ozone sonde data. All authors contributed to the writing of the manuscript.

Acknowledgements. All data used in this paper can be obtained from the contact author. This work has been supported by NIWA as part of its Government-funded, core research from New Zealand's Ministry of Business, Innovation, and Employment (MBIE). We would like to thank the Lauder team for providing most of the



440 measurements used here. We particularly thank Dan Smale for his help with various aspects of this work.
We acknowledge NOAA for the FPH data. We acknowledge ECMWF for provision of the ERA-Interim data.
We acknowledge CSIRO Marine and Atmospheric Research and the Australian Bureau of Meteorology for
the Cape Grim methane measurements. CSIRO and the Australian Bureau of Meteorology give no warranty
regarding the accuracy, completeness, currency or suitability for any particular purpose and accept no liability
445 in respect of data. We acknowledge the U.K. Met Office for use of the MetUM. Furthermore, we acknowledge
the contribution of NeSI high-performance computing facilities to the results of this research. NZ's national
facilities are provided by the NZ eScience Infrastructure and funded jointly by NeSI's collaborator institutions
and through MBIE's Infrastructure programme (<https://www.nesi.org.nz>).



References

- 450 Bodeker, G. E., Boyd, I. S., and Matthews, W. A.: Trends and variability in vertical ozone and temperature profiles measured by ozonesondes at Lauder, New Zealand: 1986-1996, *J. Geophys. Res.*, 103, 28,661-28,681, 1998.
- Boyd, I. S., Parrish, A. D., Froidevaux, L., von Clarmann, T., Kyrölä, E., Russell III, J. M., and Zawodny, J. M.: Ground-based microwave ozone radiometer measurements compared with Aura-MLS v2.2 and other
455 instruments at two Network for Detection of Atmospheric Composition Change sites, *J. Geophys. Res.*, 112, D24S33, doi:10.1029/2007JD008720, 2007.
- Carver, G., Brown, P., and Wild, O.: The ASAD atmospheric chemistry integration package and chemical reaction database, *Comput. Phys. Comm.*, 105, 197–215, 1997.
- Cunnold, D., et al.: In situ measurements of atmospheric methane at GAGE/AGAGE sites during 1985-2000
460 and resulting source inferences, *J. Geophys. Res. Atmos.*, 107, 4225, 2002.
- Dee, D. P., et al.: The ERA-Interim reanalysis: configuration and performance of the data assimilation system, *Quart. J. Royal Meteorol. Soc.*, 137, 553–597, 2011.
- Elshorbany, Y. F., Kleffmann, J., Hofzumahaus, A., Kurtenbach, R., Wiesen, P., Brauers, T., Bohn, B., Dorn, H.-P., Fuchs, H., Holland, F., Rohrer, F., Tillmann, R., Wegener, R., Wahner, A., Kanaya, Y., Yoshino, A.,
465 Nishida, S., Kajii, Y., Martinez, M., Kubistin, D., Harder, H., Lelieveld, J., Elste, T., Plass-Dülmer, C., Stange, G., Berresheim, H., and Schurath, U.: HO_x budgets during HO_xComp: A case study of HO_x chemistry under NO_x-limited conditions, *J. Geophys. Res. Atmos.*, 117, D03307, doi:10.1029/2011JD017008, 2012.
- Emmerson, K., Carslaw, N., Carpenter, L., Heard, D., Lee, J., and Pilling, M.: Urban atmospheric chemistry during the PUMA campaign 1: Comparison of modelled OH and HO₂ concentrations with measurements,
470 *J. Atmos. Chem.*, 52, 143–164, 2005.
- Emmerson, K. M., Carslaw, N., Carslaw, D. C., Lee, J. D., McFiggans, G., Bloss, W. J., Gravestock, T., Heard, D. E., Hopkins, J., Ingham, T., Pilling, M. J., Smith, S. C., Jacob, M., and Monks, P. S.: Free radical modelling studies during the UK TORCH campaign in summer 2003, *Atmos. Chem. Phys.*, 7, 167–181, 2007.
- Eyring, V., et al.: Overview of IGAC/SPARC Chemistry-Climate Model Initiative (CCMI) community simulations in support of upcoming ozone and climate assessments, *SPARC Newsletter*, 40, 48-66, 2013.
- Fuglestad, J., Jonson, J., and Isaksen, I.: Effects of reductions in stratospheric ozone on tropospheric chemistry through changes in photolysis rates, *Tellus B Chem. Phys. Meteorol.*, 46B, 172–192, 1994.
- Fuglestad, J. S., Jonson, J. E., Wang, W.-C., and Isaksen, I. S. A.: Atmospheric ozone as a climate gas: General circulation model simulations, chap. Responses in tropospheric chemistry to changes in UV fluxes, temperatures and water vapour densities, pp. 145–162, Springer, Berlin, Heidelberg, doi:10.1007/978-3-642-79869-6_10, 1995.
- Hall, E. G., Jordan, A. F., Hurst, D. F., Oltmans, S. J., Vömel, H., Kühnreich, B., and Ebert, V.: Advancements, measurement uncertainties, and recent comparisons of the NOAA frostpoint hygrometer, *Atmos. Meas. Tech. Discuss.*, doi:10.5194/amt-2016-160, in review, 2016.
- 485 Heard, D. E. and Pilling, M. J.: Measurement of OH and HO₂ in the troposphere, *Chem. Rev.*, 103, 5163–5198, 2003.



- Krol, M. C., Meirink, J. F., Bergamaschi, P., Mak, J. E., Lowe, D., Jöckel, P., Houweling, S., and Röckmann, T.: What can ^{14}C measurements tell us about OH?, *Atmos. Chem. Phys.*, 8, 5033–5044, doi:10.5194/acp-8-5033-2008, 2008.
- 490 Lelieveld, J., Dentener, F. J., Peters, W., and Krol, M. C.: On the role of hydroxyl radicals in the self-cleansing capacity of the troposphere, *Atmos. Chem. Phys.*, 4, 2337–2344, 2004.
- Levy, H.: Normal atmosphere: Large radical and formaldehyde concentrations predicted, *Science*, 173, 141–143, 1971.
- Liu, H., Crawford, J. H., Considine, D. B., Platnick, S., Norris, P. M., Duncan, B. N., Pierce, R. B., Chen, G.,
495 and Yantosca, R. M.: Sensitivity of photolysis frequencies and key tropospheric oxidants in a global model to cloud vertical distributions and optical properties, *J. Geophys. Res. Atmos.*, 114, d10305, 2009.
- Liu, S. C. and Trainer, M.: Response of the tropospheric ozone and odd hydrogen radicals to column ozone change, *J. Atmos. Chem.*, 6, 221–233, 1988.
- Logan, J. A., Prather, M. J., Wofsy, S. C., and McElroy, M. B. (1981), Tropospheric chemistry: A global perspective, *J. Geophys. Res.*, 86(C8), 7210–7254, doi:10.1029/JC086iC08p07210, 1981.
- 500 López Comí, L.: Single-column model analysis of available NIWA observations to determine the self-cleaning capacity of the atmosphere, PhD thesis, U. Canterbury, Christchurch, 2016.
- Madronich, S. and Granier, C.: Impact of recent total column ozone change on tropospheric ozone photodissociation, hydroxyl radicals, and methane trends, *Geophys. Res. Lett.*, 19, 465–467, 1992.
- 505 Manning, M., Lowe, D., Moss, R., Bodeker, G., and Allan, W.: Short-term variations in the oxidizing power of the atmosphere, *Nature*, 436, 1001–1004, 2005.
- Meinshausen, M., Smith, S. J., Calvin, K. V., Daniel, J. S., Kainuma, M. L. T., Lamarque, J.-F., Matsumoto, K., Montzka, S., Raper, S., Riahi, K., Thomson, A. M., Velders, G. J. M., and van Vuuren, D. P.: The RCP greenhouse gas concentrations and their extensions from 1765 to 2300, *Climatic Change*, 109, 213–241,
510 doi:10.1007/s10584-011-0156-z, 2011.
- Miloshevich, L., Vömel, H., Paukkunen, A., Heymsfield, A., and Oltmans, S.: Characterization and correction of relative humidity measurements from Vaisala RS80–A radiosondes at cold temperatures, *J. Atmos. Ocean. Technol.*, 18, 135–156, 2001.
- Montzka, S. A., Krol, M., Dlugokencky, E., Hall, B., Jöckel, P., and Lelieveld, J.: Small interannual variability
515 of global atmospheric hydroxyl, *Science*, 331, 67–69, 2011.
- Morgenstern, O., Braesicke, P., O'Connor, F. M., Bushell, A. C., Johnson, C. E., Osprey, S. M., and Pyle, J. A.: Evaluation of the new UKCA climate-composition model – Part I: The stratosphere, *Geosci. Model Dev.*, 2, 43–57, doi:10.5194/gmd-2-43-2009, 2009.
- Morgenstern, O., et al.: Long-range correlations in Fourier transform infrared, satellite, and modeled CO in the
520 Southern Hemisphere, *J. Geophys. Res.*, 117, D11301, doi:10.1029/2012JD017639, 2012.
- Morgenstern, O., Zeng, G., Abraham, N. L., Telford, P. J., Braesicke, P., Pyle, J. A., Hardiman, S. C., O'Connor, F. M., and Johnson, C. E.: Impacts of climate change, ozone recovery, and increasing methane on surface ozone and the tropospheric oxidizing capacity, *J. Geophys. Res. Atmos.*, 118, 1028–1041, doi:10.1029/2012JD018382, 2013.



- 525 Naik, V., et al.: Preindustrial to present-day changes in tropospheric hydroxyl radical and methane lifetime from the Atmospheric Chemistry and Climate Model Intercomparison Project (ACCMIP), *Atmos. Chem. Phys.*, 13, 5277–5298, doi:10.5194/acp-13-5277-2013, 2013.
- Nedoluha, G. E., Boyd, I. S., Parrish, A., Gomez, R. M., Allen, D. R., Froidevaux, L., Connor, B. J., and Querel, R. R.: Unusual stratospheric ozone anomalies observed in 22 years of measurements from Lauder, New Zealand, *Atmos. Chem. Phys.*, 15, 6817–6826, doi:10.5194/acp-15-6817-2015, 2015.
- 530 Neu, J. L., Prather, M. J., and Penner, J. E.: Global atmospheric chemistry: Integrating over fractional cloud cover, *J. Geophys. Res. Atmos.*, 112, D11306, doi:10.1029/2006JD008007, 2007.
- O'Connor, F. M., Johnson, C. E., Morgenstern, O., Abraham, N. L., Braesicke, P., Dalvi, M., Folberth, G. A., Sanderson, M. G., Telford, P. J., Voulgarakis, A., Young, P. J., Zeng, G., Collins, W. J., and Pyle, J. A.: Evaluation of the new UKCA climate-composition model – Part 2: The Troposphere, *Geosci. Model Dev.*, 7, 41–91, 2014.
- 535 O'Connor, F. M., Johnson, C. E., Morgenstern, O., and Collins, W. J.: Interactions between tropospheric chemistry and climate model temperature and humidity biases, *Geophys. Res. Lett.*, 36, L16801, 2009.
- Pan, L., Edwards, D. P., Gille, J. C., Smith, M. W., and Drummond, J. R.: Satellite remote sensing of tropospheric CO and CH₄: forward model studies of the MOPITT instrument, *Appl. Opt.*, 34, 30, 6976–6988, doi:10.1364/AO.34.006976, 1995.
- Pöschl, U., von Kuhlmann, R., Poisson, N., and Crutzen, P. J.: Development and intercomparison of condensed isoprene oxidation mechanisms for global atmospheric modeling, *J. Atmos. Chem.*, 37, 29–52, 2000.
- Prinn, R.: Evidence for substantial variations of atmospheric hydroxyl radicals in the past two decades, *Science*, 293, 1048, 2001.
- 545 Prinn, R., Huang, J., Weiss, R., Cunnold, D., Fraser, P., Simmonds, P., McCulloch, A., Harth, C., Reimann, S., Salameh, P., O'Doherty, S., Wang, R., Porter, L., Miller, B., and Krummel, P.: Evidence for variability of atmospheric hydroxyl radicals over the past quarter century, *Geophys. Res. Lett.*, 32, L07809, 2005.
- Rayner, N. A., Parker, D. E., Horton, E. B., Folland, C. K., Alexander, L. V., Rowell, D. P., Kent, E. C., and Kaplan, A.: Global analyses of sea surface temperature, sea ice, and night marine air temperature since the late nineteenth century, *J. Geophys. Res.*, 108, D14, 4407, doi:10.1029/2002JD002670, 2003.
- 550 Rinsland, C. P., et al.: Northern and southern hemisphere groundbased infrared spectroscopic measurements of tropospheric carbon monoxide and ethane, *J. Geophys. Res.*, 103, 28,197–28,218, 1998.
- Spivakovsky, C. M., Logan, J. A., Montzka, S. A., Balkanski, Y. J., Foreman-Fowler, M., Jones, D. B. A., Horowitz, L. W., Fusco, A. C., Brenninkmeijer, C. A. M., Prather, M. J., Wofsy, S. C., and McElroy, M. B.: Three-dimensional climatological distribution of tropospheric OH: Update and evaluation, *J. Geophys. Res. Atmos.*, 105, 8931–8980, 2000.
- Stevenson, D., Johnson, C., Collins, W., Derwent, R., and Edwards, J.: Future estimates of tropospheric ozone radiative forcing and methane turnover – the impact of climate change, *Geophys. Res. Lett.*, 27, 2073–2076, 2000.
- 560 Stevenson, D., et al.: Multimodel ensemble simulations of present-day and near-future tropospheric ozone, *J. Geophys. Res. Atmos.*, 111, D08301, 2006.



- Stone, K. A., Morgenstern, O., Karoly, D. J., Klekociuk, A. R., French, W. J., Abraham, N. L., and Schofield, R.:
Evaluation of the ACCESS – chemistry–climate model for the Southern Hemisphere, *Atmos. Chem. Phys.*,
565 16, 2401–2415, doi:10.5194/acp-16-2401-2016, 2016.
- Tang, Y., Carmichael, G. R., Uno, I., Woo, J.-H., Kurata, G., Lefer, B., Shetter, R. E., Huang, H., Anderson,
B. E., Avery, M. A., Clarke, A. D., and Blake, D. R.: Impacts of aerosols and clouds on photolysis frequen-
cies and photochemistry during TRACE-P: 2. Three-dimensional study using a regional chemical transport
model, *J. Geophys. Res. Atmos.*, 108, 8822, 2003.
- 570 Telford, P. J., Abraham, N. L., Archibald, A. T., Braesicke, P., Dalvi, M., Morgenstern, O., O’Connor,
F. M., Richards, N. A. D., and Pyle, J. A.: Implementation of the Fast-JX Photolysis scheme (v6.4) into
the UKCA component of the MetUM chemistry–climate model (v7.3), *Geosci. Model Dev.*, 6, 161–177,
doi:10.5194/gmd-6-161-2013, 2013.
- Thompson, A. M.: The oxidizing capacity of the Earth’s atmosphere: Probable past and future changes, *Science*,
575 256, 1157–1165, 1992.
- Thompson, A. M., Stewart, R. W., Owens, M. A., and Herwehe, J. A.: Sensitivity of tropospheric oxidants to
global chemical and climate change, *Atmos. Environ.*, 23, 519–532, 1989.
- Tie, X., Madronich, S., Walters, S., Zhang, R., Rasch, P., and Collins, W.: Effect of clouds on photolysis and
oxidants in the troposphere, *J. Geophys. Res. Atmos.*, 108, 4642, 2003.
- 580 Vömel, H., David, D. E., and Smith, K.: Accuracy of tropospheric and stratospheric water vapor measurements
by the cryogenic frost point hygrometer: Instrumental details and observations, *J. Geophys. Res.*, 112, 8305,
doi:10.1029/2006JD007224, 2007.
- Wild, O.: Modelling the global tropospheric ozone budget: exploring the variability in current models, *Atmos.*
Chem. Phys., 7, 2643–2660, 2007.
- 585 WMO: Scientific Assessment of Ozone Depletion: 2010, WMO Global Ozone Research and Monitoring Project
– Report No 52, Geneva, Switzerland, 2011.
- Zeng, G., Pyle, J. A., and Young, P. J.: Impact of climate change on tropospheric ozone and its global budgets,
Atmos. Chem. Phys., 8, 369–387, doi:10.5194/acp-8-369-2008, 2008.
- Zeng, G., Wood, S. W., Morgenstern, O., Jones, N. B., Robinson, J., and Smale, D.: Trends and variations in
590 CO, C₂H₆, and HCN in the Southern Hemisphere point to the declining anthropogenic emissions of CO
and C₂H₆, *Atmos. Chem. Phys.*, 12, 7543–7555, doi:10.5194/acp-12-7543-2012, 2012.

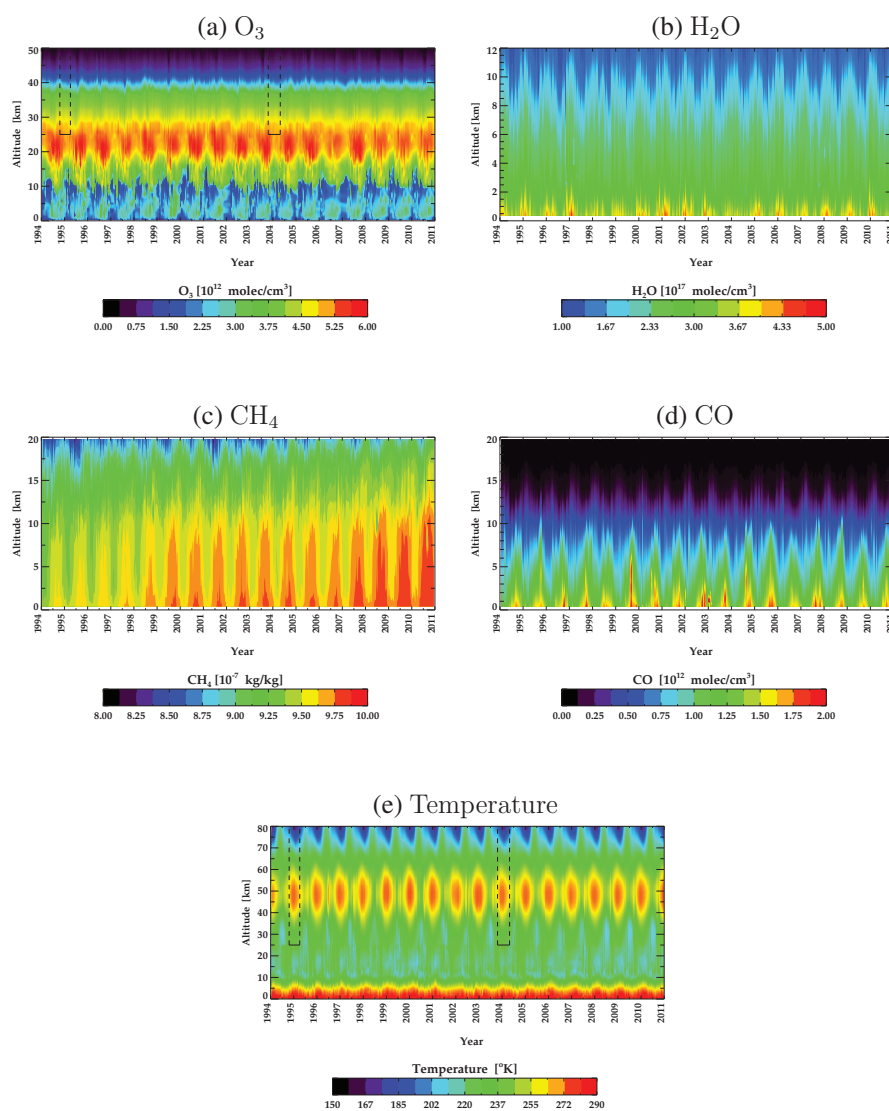


Figure 1. (a) Time series of O_3 profiles constructed by ozonesonde measurements spliced with MOPII measurements. (b) Time series of H_2O profiles constructed by radiosonde measurements spliced with NIWA-UKCA H_2O (time series of ERAI – NIWA-UKCA H_2O is not displayed here). (c) Time series of CH_4 profiles constructed by rescaling the NIWA-UKCA CH_4 to surface CH_4 measurements from Cape Grim (Tasmania). (d) Time series of CO profiles constructed by rescaling the NIWA-UKCA CO to CO measurements from the FTIR spectrometer. (e) Time series of temperature profiles constructed by radiosonde measurements merged with MOPII measurements. The areas within black boxes were filled using a Fourier series gap filling method.

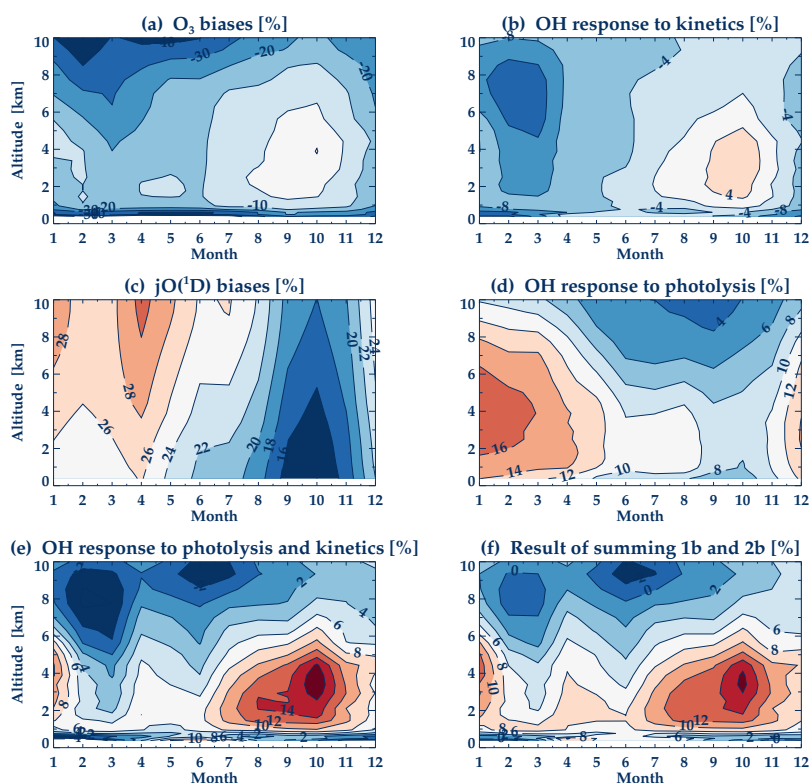


Figure 2. Multi-annual and monthly-mean OH responses to O₃ biases between observations and the reference simulation. (a) Difference in O₃ (%) relative to the reference simulation. (b) OH difference (%) relative to the reference simulation accounting only for the kinetics effects of O₃ differences (e.g. with $j\text{O}(^1\text{D})$ unchanged). (c) Difference in $j\text{O}(^1\text{D})$ (%) relative to the reference simulation. (d) OH difference (%) relative to the reference simulation accounting only for $j\text{O}(^1\text{D})$ differences (e.g. with O₃ unchanged). (e) OH differences relative to the reference simulation considering the combined kinetics and photolysis effects. (f) Sum of (b) and (d).



Forcings	Data used
O ₃	1. Kinetics effect: O ₃ changes → ozonesondes (0-25 km) + MOPII (26-84 km) NIWA-UKCA data for other species and temperature 2. Photolysis effect: j_{O^1D} changes according to O ₃ changes NIWA-UKCA data for all species and temperature 3. Kinetics + photolysis effects: O ₃ changes → ozonesondes + MOPII j_{O^1D} changes according to O ₃ changes NIWA-UKCA data for other species and temperature
H ₂ O	1. Changes in H ₂ O → radiosondes (0-8 km) + NIWA-UKCA H ₂ O (9-84 km) NIWA-UKCA data for other species and temperature 2. Changes in H ₂ O → ERAI (0-8 km) + NIWA-UKCA H ₂ O (9-84 km) NIWA-UKCA data for other species and temperature.
CH ₄	Changes in CH ₄ → rescaled NIWA-UKCA CH ₄ to Cape Grim surface CH ₄ NIWA-UKCA data for other species and temperature.
CO	Changes in CO → rescaled NIWA-UKCA CO profiles to FTIR CO NIWA-UKCA data for other species and temperature
<i>T</i>	1. Kinetics effect: temperature changes → radiosondes (0-25 km) + MOPII (26-84 km) NIWA-UKCA data for all species 2. Photolysis effect: j_{O^1D} changes according to temperature changes NIWA-UKCA data for all species and temperature 3. Kinetics + photolysis effects: temperature changes → radiosondes + MOPII j_{O^1D} changes according to temperature changes NIWA-UKCA data for all species
O ₃ , H ₂ O, CH ₄ , CO, <i>T</i>	Changes in O ₃ , H ₂ O, CH ₄ , CO, and temperature using observations mentioned above For H ₂ O, radiosonde (0-8 km) + NIWA-UKCA (9-84 km) data are used
Reference	NIWA-UKCA data for all species and temperature

Table 1. Sensitivity simulations performed with the SCM to assess the contribution of changes in the key forcings to OH chemistry at Lauder under clear-sky conditions. The table includes the type of measurement/data set used to prescribe the key forcings. The time period of simulation is between 1994 and 2010.

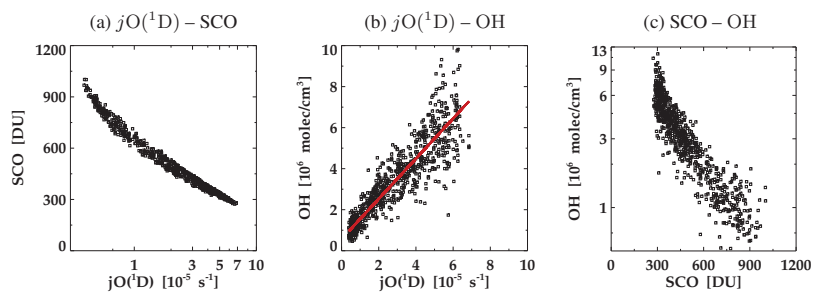


Figure 3. (a) Scatter plots of the approximately exponential relationship of $jO(^1D)$ with the slant column O_3 (SCO). (b) Linear relationship of $jO(^1D)$ and the OH concentration. The red solid line denotes the linear fit between them. (c) Exponential relationship of the SCO with the OH concentration. The results shown in this figure are those obtained from the combined simulation (kinetics and photolysis effects).

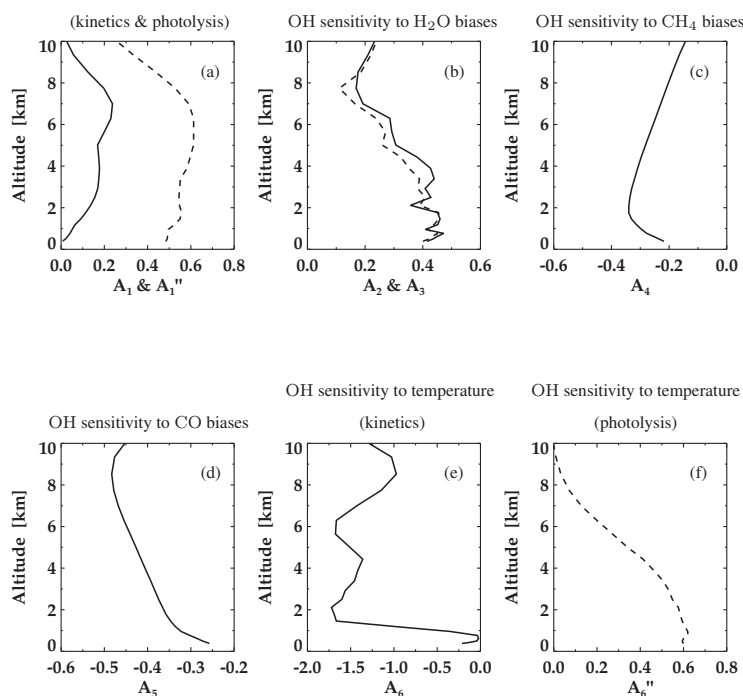


Figure 4. Sensitivity coefficients ' A_i ' between OH and each perturbation variable: In the calculation, multi-annual mean relative differences in OH and in the forcing are ratioed. (a) Sensitivity of OH to changes in O_3 levels (kinetics effect) denoted by A_1 (solid line) and to changes in $jO(^1D)$ due to changes in O_3 (photolysis effect) denoted by A_1'' (dashed line); (b) sensitivity of OH to changes in radiosonde – NIWA-UKCA CCM H_2O (A_2 solid line) and to changes in ERAI – NIWA-UKCA H_2O (A_3 dashed line); (c) sensitivity of OH to changes in CH_4 (A_4); (d) sensitivity of OH to changes in CO (A_5); (e) sensitivity of OH to changes in temperature (kinetics effect) denoted by A_6 ; (f) sensitivity of OH to changes in $jO(^1D)$ due to changes in temperature (photolysis effect) denoted by A_6'' .

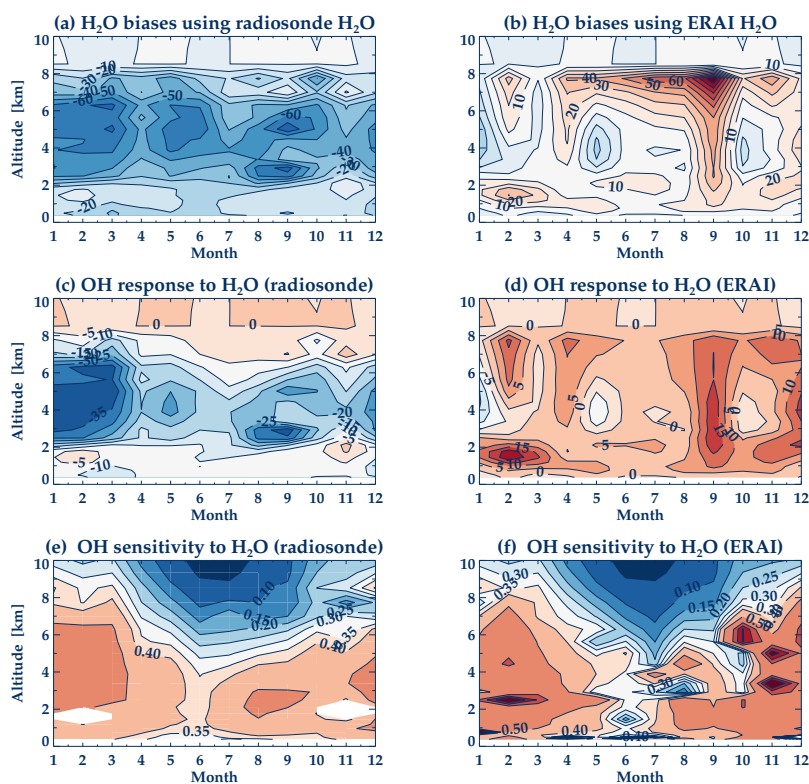


Figure 5. Multi-annual and monthly-mean OH responses to H₂O between perturbation simulations and the reference simulation. (a) Difference in radiosonde – NIWA-UKCA H₂O (%) relative to the reference simulation. (b) Difference in ERAI – NIWA-UKCA H₂O (%) relative to the reference simulation. (c) OH difference (%) relative to the reference simulation using radiosonde – NIWA-UKCA H₂O. (d) OH difference (%) relative to the reference simulation using ERAI – NIWA-UKCA CCM H₂O. (e) Ratio of OH changes to changes in H₂O expressed as $\frac{\partial \ln \text{OH}}{\partial \ln \text{H}_2\text{O}}$. (f) Ratio of OH changes to changes in H₂O expressed as $\frac{\partial \ln \text{OH}}{\partial \ln \text{H}_2\text{O}}$. Above 8 km NIWA-UKCA H₂O was used in both cases. Therefore, differences with respect to the reference simulation are close to 0.

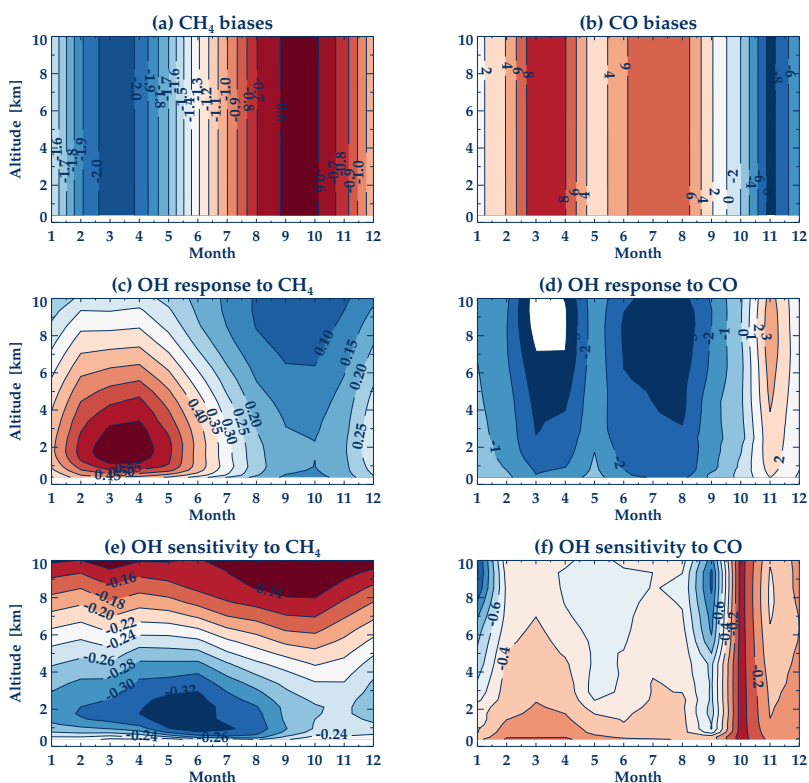


Figure 6. Multi-annual and monthly-mean OH responses to CH₄ and CO biases between observations and the reference simulation. (a) Difference in CH₄ (%) relative to the reference simulation. (b) Difference in CO (%) relative to the reference simulation. (c) OH difference (%) relative to the reference simulation according to CH₄ biases. (d) OH difference (%) relative to the reference simulation according to CO biases. (e) Ratio of OH changes to changes in CH₄ expressed as $\frac{\partial \ln \text{OH}}{\partial \ln \text{CH}_4}$. (f) Ratio of OH changes to changes in CO expressed as $\frac{\partial \ln \text{OH}}{\partial \ln \text{CO}}$.

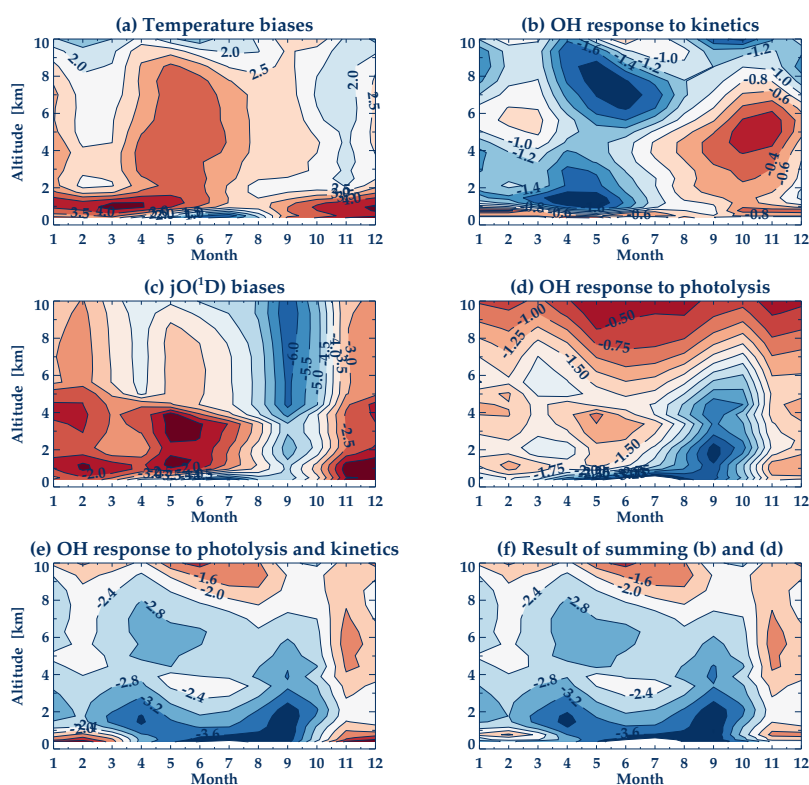


Figure 7. Multi-annual and monthly-mean OH responses to temperature biases between observations (radiosonde – MOPI1 temperature) and the reference simulation. (a) Difference in radiosonde – MOPI1 temperature (K) relative to the reference temperature. (b) OH difference (%) relative to the reference simulation accounting only for the kinetics effects of temperature differences (e.g. with $j\text{O}(^1\text{D})$ unchanged). (c) Difference in $j\text{O}(^1\text{D})$ (%) relative to the reference simulation. (d) OH difference (%) relative to the reference simulation accounting only for $j\text{O}(^1\text{D})$ differences (i.e. with temperature unchanged). (e) OH differences relative to the reference simulation considering the combined kinetics and photolysis effects. (f) Sum of (b) and (d).

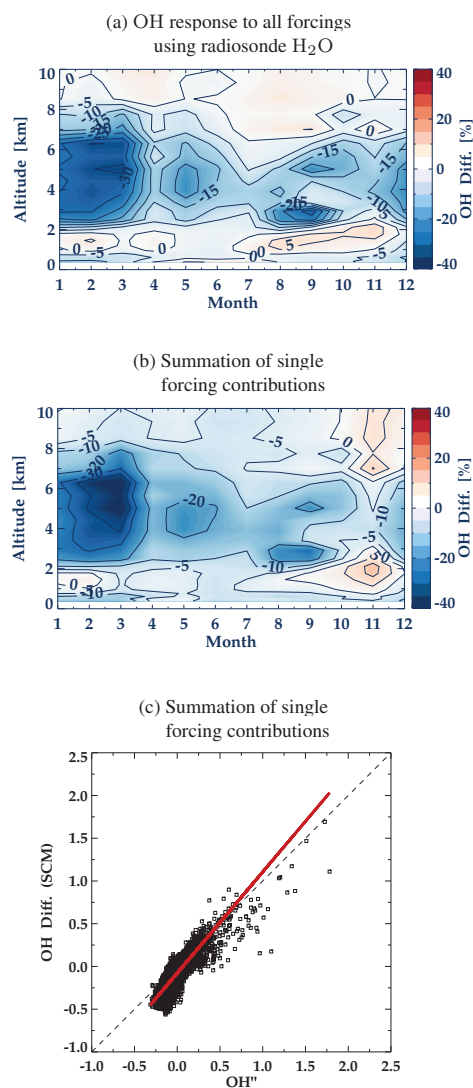


Figure 8. (a) Multi-annual and monthly-mean percentage difference in OH between a simulation with bias-correction applied to all five fields and the reference simulation. Radiosonde H₂O is assumed below 8 km. (b) Summation of all the single forcing contributions as expressed by the right hand side of Eq. (3). Radiosonde H₂O is assumed below 8 km. (c) Scatter plot of the response of OH to the combination of all forcings (vertical axis) versus the summation of the OH response to individual forcings (horizontal axis) as expressed by the right hand side of Eq. (3) (denoted by OH^{''}).

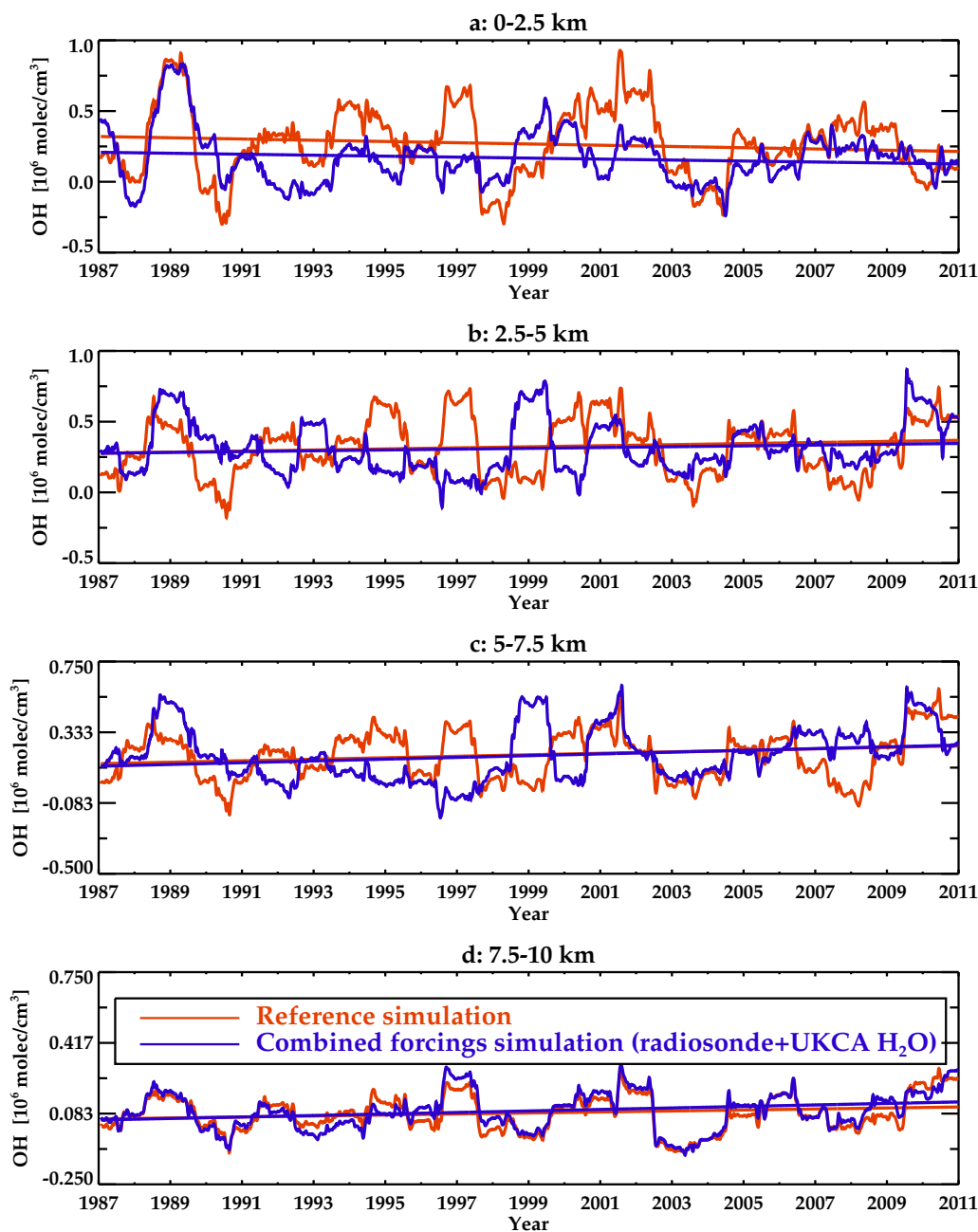


Figure 9. Variability and trends of the OH anomalies at different altitudes: (a) 0-2.5 km, (b) 2.5-5 km, (c) 5-7.5 km, and (d) 7.5-10 km. The red solid line is the time series of the reference simulation and the blue solid line is the combined forcings simulation considering radiosonde – NIWA-UKCA H₂O.

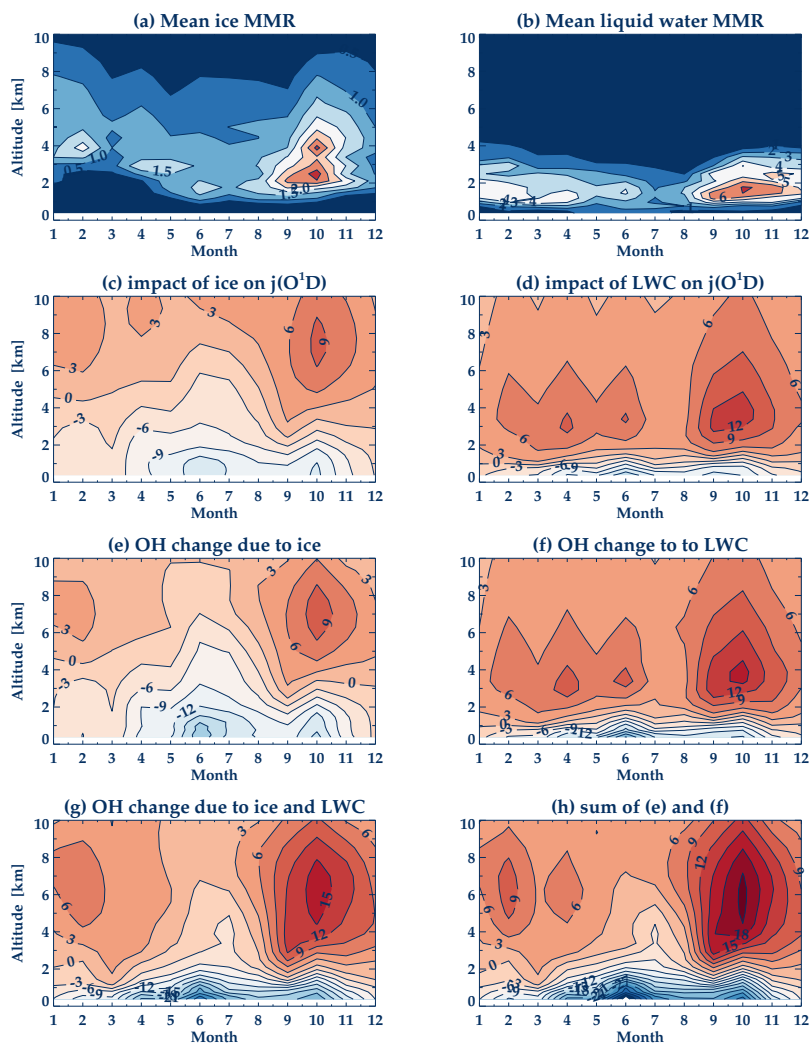


Figure 10. Multi-annual and monthly-mean OH responses to the presence of clouds. Multi-annual and monthly mean (a) ice content (kg/kg). (b) liquid water content (kg/kg). (c) Response of j_{O^1D} (%) to the presence of ICs relative to the cloud-free reference simulation. (d) response of j_{O^1D} (%) to the presence of LWCs relative to the cloud-free reference simulation. (e) response of OH (%) to the presence of ICs relative to the cloud-free reference simulation. (f) Response of OH (%) to the presence of LWCs relative to the cloud-free reference simulation. (g) response of OH (%) to the presence of both LWCs and ICs relative to the cloud-free reference simulation. (h) Sum of 3a and 3b.